Journal of Zhejiang University-SCIENCE A (Applied Physics & Engineering)
ISSN 1673-565X (Print); ISSN 1862-1775 (Online)
www.jzus.zju.edu.cn; www.springerlink.com
E-mail: jzus@zju.edu.cn

A high-capacity graphene/mesocarbon microbead composite anode for lithium-ion batteries*

Inna SMOLIANOVA[1,2], Jin-long HU[1], Xin-yue ZHAO[1], Viacheslav DEMENTIEV[3], Ling-zhi ZHANG[†‡1]

[1]*CAS Key Laboratory of Renewable Energy, Guangdong Provincial Key Laboratory of New and Renewable Energy Research and Development, Guangzhou Institute of Energy Conversion, Chinese Academy of Sciences, Guangzhou 510640, China*

[2]*University of Chinese Academy of Sciences, Beijing 100049, China*

[3]*FESCOM Technologies Ltd., Territory of the Innovation Center Skolkovo, Moscow 143026, Russia*

[†]E-mail: lzzhang@ms.giec.ac.cn

Received Nov. 24, 2019; Revision accepted Mar. 1, 2020; Crosschecked Apr. 15, 2020

Abstract: The graphene/mesocarbon microbead (MCMB) composite is assessed as an anode material with a high capacity for lithium-ion batteries. The composite electrode exhibits improved cycling stability and rate capability, delivering a high initial charge/discharge capacity of 421.4 mA·h/g/494.8 mA·h/g as well as an excellent capacity retention over 500 cycles at a current density of 40 mA/g. At a higher current density of 800 mA/g, the electrode still retains 35% of its initial capacity which exceeds the capacity retention of pure graphene or MCMB reference electrodes. Cyclic voltammetry and electrochemical impedance spectroscopy reveal that the composite electrode favors electrochemical kinetics as compared with graphene and MCMB separately. Superior electrochemical properties suggest a strong synergetic effect between highly conductive graphene and MCMB.

Key words: Graphene; Mesocarbon microbead (MCMB); Composite anode materials; Lithium-ion batteries
https://doi.org/10.1631/jzus.A1900600 **CLC number:** O646

1 Introduction

The rapid development of electronic devices and their industrial applications has created a rising demand for high energy storage devices. Rechargeable batteries are used in a wide range of applications, from industrial equipment and emergency/standby power to portable devices and electric vehicles. Among rechargeable batteries, lithium-ion batteries (LIBs) present obvious advantages in such applications because of their long working life, low self-discharge rate, and good ability to operate across a broad temperature range (Linden and Reddy, 2002; Birrozzi et al., 2015). Additionally, high energy density makes LIBs attractive for weight- or volume-sensitive applications.

Graphite is a widely used commercial anode material for LIBs due to its high coulombic efficiency and stable cycling performance at low current densities. However, the conventional graphite anode does not meet the call for higher energy storage batteries (e.g. electric vehicles), because of its limited specific capacity (Jaguemont et al., 2016) and poor power density (Dunn et al., 2011). Hence, many carbonaceous materials with different morphologies and structures have been considered as alternatives to replace graphite. Relevant examples are 0D carbon spheres (Wang et al., 2005), 1D carbon nanotubes and

‡ Corresponding author

* Project supported by the National Natural Science Foundation of China (No. 21573239), the Guangdong Provincial Project for Science and Technology (Nos. 2014TX01N14, 2015B010135008, and 2016B010114003), the Guangzhou Municipal Project for Science and Technology (No. 201509010018), and the K. C. WONG Education Foundation, China

ORCID: Inna SMOLIANOVA, https://orcid.org/0000-0002-3605-7493

nanofibers (Welna et al., 2011; Wang et al., 2013), 2D graphene oxide, reduced graphene oxide, doped graphene layers (Wu et al., 2011), and 3D carbon-carbon and carbon-metal oxide materials (Li et al., 2012; Wu et al., 2012). Among these, graphene has attracted an enormous interest owing to its large theoretical specific surface area (2630 m^2/g), excellent thermal conductivity (Zhu et al., 2010), high theoretical capacity (744 mA·h/g if based on Li_2C_6 alloy) (Cai et al., 2017), broad voltage window (Du et al., 2016), and superior flexibility and mechanical strength (Allen et al., 2010). Graphene can be produced by both physical and chemical approaches. The chemical process, based on graphite oxide reduction, is a typical synthesis technique which usually generates graphene with some hydroxyl, epoxy, and carboxyl functional groups on the surface (Compton and Nguyen, 2010). However, such oxygen-containing functional groups are one of the reasons for electrolyte decomposition caused by side reactions. Physical exfoliation uses different ways to overcome van der Waals attractions between graphite layers to produce individual graphene sheets (Cai et al., 2012). This production method is cost-effective, well-scaled and renders defect-free graphene sheets with few residual functional groups on their surfaces (Cai et al., 2017) benefiting cycling stability when used as an anode material (Novoselov et al., 2004; Yoo et al., 2008; Wang et al., 2009). However, strong interactions between individual graphene layers make them highly likely to aggregate to form powders and thus to decrease their specific surface area whilst increasing Li-ion diffusion resistance, leading to insufficient usage of the graphene layers for lithium storage. Therefore, the control of the layered structure of graphene can be a crucial principle for better electrochemical performance.

Mesocarbon microbead (MCMB) is a well-known carbonaceous anode material with spherical lamellar shaped particles (Mochida et al., 2000) and a smooth surface. Its structure ensures efficient transfer of lithium ions and reduces the side reactions of the electrolyte during the charge/discharge process (Alcántara et al., 2000) and those together result in excellent cycling stability. However, MCMB application in LIBs has been limited due to its relatively low specific capacity and unsatisfactory rate performance.

In this work, we report a novel graphene/MCMB composite as an anode material for LIBs, aiming to improve their cycling performance by using our home-made physically exfoliated graphene with high electrical conductivity (782 S/cm) and MCMB with intrinsically excellent cycling stability. MCMB with spherical morphology helps to prevent the aggregation of graphene sheets and thus facilitates condensed packing for the graphene/MCMB composite electrode. The structure of the electrode, along with its electrochemical properties has been studied. The results are compared with reference electrodes of graphene and MCMB.

2 Methods

2.1 Reagents

Graphene (particle size≤20 μm, purity 99.6%) was provided by FESCOM Technologies Ltd., Russia. MCMB (particle size of 5–15 μm, purity 99.8%) was purchased from Shanshan Technology, China. Polyvinylidene fluoride (PVDF) (Solvay Solef® 6020, purity 99.9%) was purchased from Shenzhen Micro Electron Co., China. N-methyl-2-pyrrolidone (NMP) (99.99% purity) was purchased from Aladdin Industrial Co., China. Electrolyte 1 mol/L $LiPF_6$ in ethylene carbonate (EC)/dimethyl carbonate (DMC)/ethyl methyl carbonate (EMC) (V_{EC}:V_{DMC}:V_{EMC}= 1:1:1) was purchased from Zhangjiagang Guotai-Huarong New Chemical Materials Co., China. All the reagents were used without further purification.

2.2 Materials and electrochemical characterization

The morphology and structure of the raw materials and electrodes were characterized by scanning electron microscopy (SEM) (Hitachi S-4800, Japan). Graphene conductivity at room temperature was tested by the four-probe method (SDY-4 measurement system, Guangzhou 4 probes Tech, China) after being pressed to a pellet at 10 MPa.

The composite material was prepared by mechanical mixing (mortar milling for 1 h) of graphene and MCMB in weight ratios of 7:3, 8:2, and 9:1. The composite electrodes, which will be further denoted as GMC (7:3), GMC (8:2), and GMC (9:1) according to their weight ratios, along with reference electrodes of graphene and MCMB, were prepared by mixing the active material, conducting agent (acetylene

black), and PVDF binder in a 90:5:5 weight ratio. NMP was used as the solvent. The slurry was coated on copper foil, which acted as both the substrate and the current collector. The loading level for all the electrodes was kept at around 1.2–1.4 mg/cm. The electrodes were dried for 24 h at 110 °C under vacuum. Coin type half cells (CR2025) were assembled in the Ar-filled glove box (water and an oxygen content<0.1×10^{-6}) using 1 mol/L $LiPF_6$ (V_{EC}:V_{DMC}:V_{EMC} =1:1:1) as an electrolyte, lithium metal as a counter electrode, and Celgard 2400 polypropylene membrane as a separator. The specific capacities were calculated based on the total mass of the composites. Galvanostatic charge/discharge was conducted at various current rates in a voltage window between 0.01 and 3.5 V (vs Li/Li^+) at Shenzhen Neware Battery Cycler, China. Electrochemical impedance spectroscopy (EIS) and cyclic voltammetry (CV) were measured using an IM6e electrochemical workstation (Zahner, Germany). CV was carried out between 0.01 and 3.5 V at 0.3 mV/s scanning speed. EIS was conducted in a frequency range between 10 mHz and 100 kHz with amplitude of 5 mV.

3 Results and discussion

The morphology and microstructure of raw graphene powder, MCMB, and the electrode sheets of neat graphene and GMC were observed by SEM. Graphene powder shows a sheet-shaped structure with some crumples and wrinkles with non-uniform particle size distribution varying from 2 to 50 μm (Fig. 1a). Graphene sheets stack together with a thickness of 5–7 nm (about 10–20 layers (Guo et al., 2009)), and further agglomerate forming clusters of approximately 200–300 nm thick, creating big structural voids (Fig. 1b). The electrical conductivity was measured to be 782 S/cm by using a 4-point probe apparatus. MCMB displays a uniform spherical shape with particle size varying from 5 to 15 μm (Fig. 1c). After the processing of electrode slurry, the structure of the graphene reference electrode remains unchanged, preserving the cavities between clusters (Fig. 1d). To circumvent this particular difficulty, MCMB was chosen as an additive to graphene; three different weight ratios of graphene/MCMB ((7:3), (8:2), (9:1)) were prepared for comparison. The SEM images of GMC (8:2) (Figs. 1e and 1f) demonstrate how MCMB fills in the structural voids between graphene clusters, resulting in a higher density electrode packing, which can consequently increase the conductivity of the electrode sheet and enlarge the electrode/electrolyte surface for lithium storage.

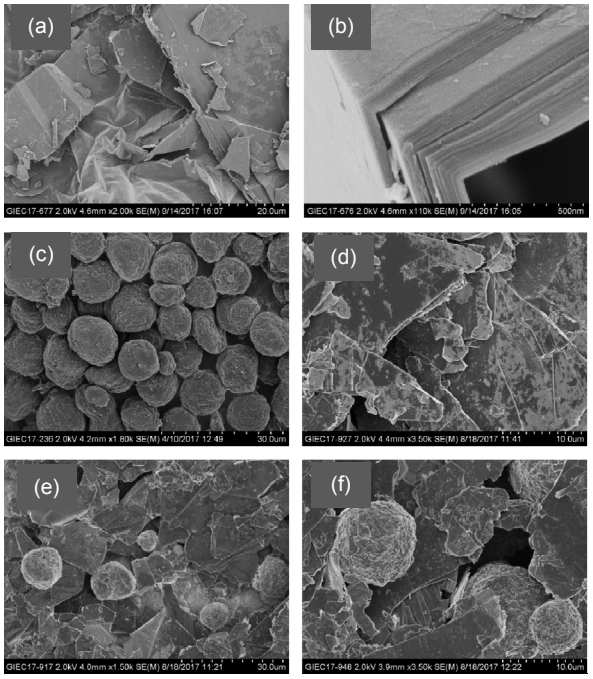

Fig. 1 SEM images of graphene powder (a), graphene sheet (b), MCMB (c), graphene electrode (d), and GMC (8:2) at magnifications of 1500 (e) and 3500 (f)

Galvanostatic charge/discharge was performed at a current density of 40 mA/g (approximately 0.1 C since one charge (discharge) is completed in approximately 10 h) (Fig. 2a). The first charge/discharge capacity and coulombic efficiency for the graphene reference electrode are 348.93 mA·h/g/421.8 mA·h/g and 82.7%, and for the MCMB reference electrode 311.6 mA·h/g/348.0 mA·h/g and 89.6%, respectively. Accordingly, GMC electrodes were expected to obtain specific capacities between reference values. The GMC (7:3), GMC (8:2), and GMC (9:1) electrodes present a first charge/discharge capacity of 314.3/365.0, 421.4/494.8, and 398.8 mA·h/g/460.5 mA·h/g, respectively. The initial coulombic efficiencies are calculated to be 86.1%, 85.1%, and 86.6%, respectively. Thus, the specific capacity values for GMC (8:2) and GMC (9:1) exceed the calculated values (21.5% higher for GMC (8:2) and

11% for GMC (9:1)), while the experimental value of GMC (7:3) is 8.5% lower. The graphene reference electrode and the GMC electrodes show a minor capacity enhancement during the cycling. After 100 cycles the graphene reference electrode delivers a reversible capacity of 411.1 mA·h/g and 97.5% of capacity retention. GMC (7:3) exhibits a specific capacity of 402.0 mA·h/g which is 10% higher than the initial capacity of the cell. GMC (9:1) and GMC (8:2) deliver specific capacities of 447.9 mA·h/g and 459.3 mA·h/g which refer to capacity retentions of 97.3% and 92.8%, respectively. Due to the superior capacity values of GMC (8:2), it was chosen to carry out the electrochemical tests as discussed hereafter.

The rate performance was measured at different current densities from 40 to 800 mA/g; over the final 15 cycles, the current density was set back to 40 mA/g (Fig. 2b). The corresponding reversible capacities for GMC (8:2) are 440.1, 407.6, 353.5, 258.5, and 153.0 mA·h/g at current densities of 40, 100, 200, 400, and 800 mA/g, respectively. At the same current densities, graphene and MCMB reference electrodes can deliver 350.7, 304.6, 261.3, 169.2, 74.4 mA·h/g and 272.0, 245.0, 134.0, 47.4, 20.3 mA·h/g, respectively. At a current density of 800 mA/g, GMC (8:2) retains 35% of its capacity which is higher than the values obtained for graphene and MCMB electrodes (21% and 7%, respectively). When the current density is set back to 40 mA·/g, all the three anodes reached 100% capacity retention, i.e. an indication of high structural stability and excellent electrochemical reversibility. The enhanced rate performance of GMC (8:2) in comparison to the reference electrodes can be attributed to the improved electrode morphology, which enables lithium transport to the active material due to faster electrolyte diffusion into the inner areas (Collins et al., 2015).

Charge/Discharge profiles of the three electrodes (graphene, MCMB, GMC (8:2)) at the first cycle in a voltage range of 0.01–3.5 V (vs. Li^+/Li) are shown in Fig. 3a. Charge/Discharge curves with a flat broad plateau below 0.1 V are typical for carbonaceous materials and plateaus are ascribed to lithium intercalation (or extraction) into active material and forming LiC_6 alloy. The plateau of the GMC (8:2) electrode is broader than that for reference electrodes, which indicates more effective lithium

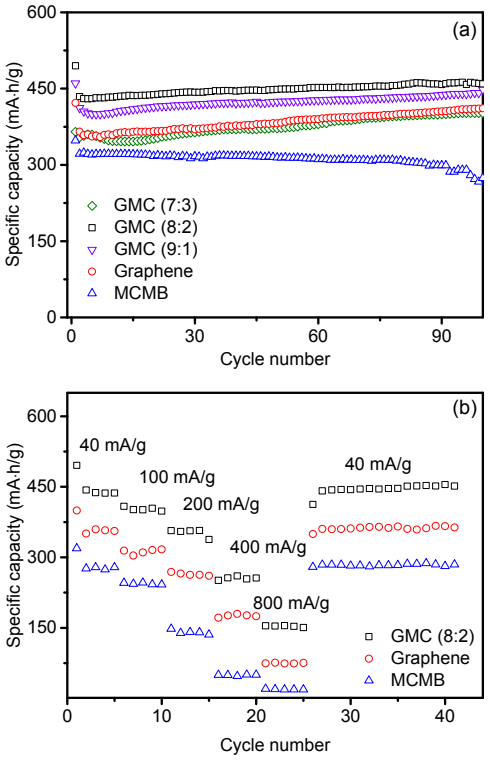

Fig. 2 Cycling performance of graphene, MCMB, GMC (9:1), GMC (8:2), GMC (7:3) electrodes at 40 mA/g (a) and GMC (8:2), graphene, and MCMB electrodes at different current densities (b)

storage. Broad sloped plateaus at the discharge curve at 0.5–1.75 V are attributed to the solid electrolyte interphase (SEI) formation (Yao et al., 2003; Wang et al., 2016; Imtiaz et al., 2017) and disappear after the first cycle. The significant difference among electrodes appears in the charge curves on the region above 0.25 V. Graphene and MCMB reference electrodes do not show any significant capacity increase in the region as can be seen from the close to vertical slope. As comparison, the charge curve of GMC (8:2) has a slope starting about 0.25 V, which indicates the existence of new ways of accommodation for lithium in the composite material (Hu et al., 2007). The charge/discharge profiles of GMC (8:2) electrode at the 1st, 2nd, 100th, 300th, and 500th cycle (Fig. 3b) can provide clarification of lithium storage mechanisms in the composite material and are the possible reason behind capacity enhancement during cycling. Charge curves have a shape similar to those observed in hard carbons (Hu et al., 2007) and consist of four regions: (1) a plateau below 0.25 V attributed to the

lithium deposition in micropores (Peled et al., 1998); (2) a slope at 0.25–1.0 V attributed to the lithium intercalation between disordered graphite layers (Dahn et al., 1995); (3) a sloped plateau at 1.0–2.6 V attributed to lithium binding into hydrogen-terminated dangling bonds (Wang et al., 1999); (4) a sloped curve above 2.6 V attributed to partial decomposition of SEI at high voltage. The contribution of regions (2)–(4) to the specific capacity of the GMC electrode grows with cycling. The capacity increment in region (2) indicates the enhanced lithium intercalation between graphene layers. Increased lithium binding into hydrogen-terminated lithium bonds (region (3)) is explained by the reversible forming/breaking of C-H bonds (Ogumi and Inaba, 1998) and the formation of new dangling bonds upon cycling. The decomposition of SEI (region (4)) indicates that some of its components are unstable upon charging and their decomposition contributes towards reversible capacity (Ogumi and Inaba, 1998). Discharge curves show the evolution of the 0.25–1.75 V plateau from the 2nd to the 500th cycle. Slope changes at the discharge curve can be assigned to differences in grain size, as well as increased disorder in the electrode material and at geometrically nonequivalent lithium storage sites (Yun et al., 2014). Thus, the increase of the specific capacity with cycling can be attributed to the gradual activation of the electrode. Similar behavior was previously described for a number of carbonaceous electrodes (Qie et al., 2012; Zhu et al., 2016; Liu et al., 2018; Li et al., 2019;Wang et al., 2019; Zhao et al., 2019)

Dispersion properties of graphene, MCMB, and GMC (8:2) in PVDF binder were evaluated by the Scratch method (Fig. 4). The length of the uniform dispersion region for MCMB is more than twice the length of that for graphene (32.5 vs. 12.5 units), while GMC (8:2) shows 27.5 units of uniform region length. Poor dispersion characteristics of neat graphene with PVDF binder might be the main reason behind the low capacity of the graphene reference electrode. Visual evaluation proves that poor dispersibility can be significantly improved by the addition of MCMB.

To clarify the importance of the addition of the second component to graphene for improving both specific capacity and cycling stability of the graphene electrode, a comparison experiment was

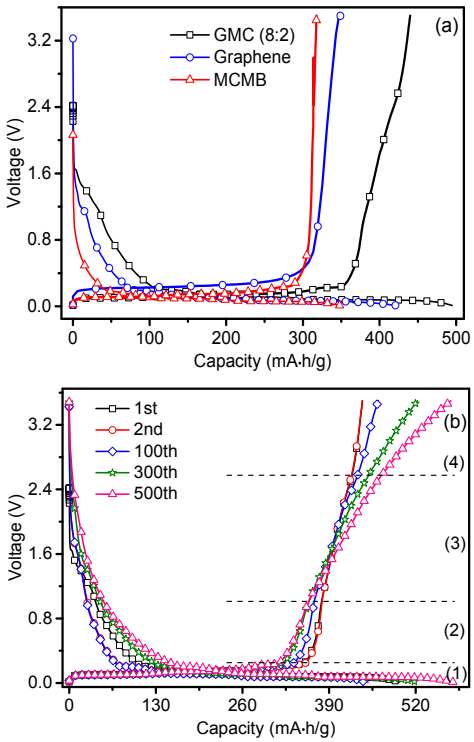

Fig. 3 Charge/Discharge profiles for the initial cycle of graphene, MCMB, and GMC (8:2) electrodes (a) and the 1st, 2nd, 100th, 300th, 500th cycles of the GMC (8:2) electrode (b)

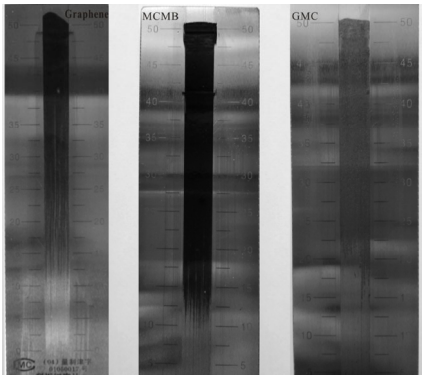

Fig. 4 Dispersion properties of graphene, MCMB, and GMC (8:2) in PVDF binder

conducted by using an anode with 95% graphene and 5% PVDF (Fig. 5a). It is worth noting that the graphene used in this work has a very high conductivity of 782 S/cm; thus, the conducting agent may not be necessary for processing the electrode sheet. These results are compared with the graphene reference electrode. The initial charge/discharge capacities of a graphene cell without a conducting agent are

331.35 mA·h/g/490.32 mA·h/g. The discharge capacity decreases to 199.0 mA·h/g after 112 cycles and then gradually increases to a value of 261.9 mA·h/g at the 270th cycle. As a comparison, the graphene reference electrode (with AB conducting agent) shows a slightly decreased discharge capacity of 354.7 mA·h/g after seven cycles and then gradually increases to a value of 458.7 mA·h/g at the 270th cycle. Both the specific capacity and cycling stability of the graphene cell without a conducting agent are poorer than those of the graphene reference electrode.

The GMC electrodes show a strong synergetic effect between graphene and MCMB. Poor dispersibility of graphene powder in the PVDF binder is significantly improved with the addition of MCMB. It is found that the large size of pristine graphene particles results in large voids and poor contact between them, and those have an adverse effect on the electrical conductivity. MCMB fills in the voids, providing better electrical contact and enlarging the electrode/electrolyte surface for lithium storage. Among composite electrodes, GMC (8:2) shows the best electrochemical performance. A combination of 80% of graphene and 20% of MCMB also provides more condensed packing of the electrode (in comparison with GMC (9:1)), while GMC (7:3) electrode has lower capacity due to excessive MCMB content. Similar results were observed by Yao et al. (2003) for carbon nanotubes/graphene and fullerene/graphene composites. Therefore, it can be concluded that the introduction of the second component, especially spherical MCMB in this work, improves the electrochemical performance of graphene when used as an anode.

The cycling performance of the GMC (8:2) electrode over 500 cycles at a current density of 40 mA/g is presented in Fig. 5b. As mentioned above, the GMC electrode shows initial charge and discharge capacities of 421.4 and 494.8 mA·h/g, respectively, with an initial coulombic efficiency of 85.1%. The coulombic efficiency, however, increases to 99% after the 3rd cycle and remains close to 100% over the following 500 cycles. The GMC (8:2) electrode maintains high reversibility, reaching a capacity of 578.9 mA·h/g after 503 cycles.

CV was conducted to further investigate the lithium insertion/extraction process (Fig. 6a). A cathodic scan of the GMC (8:2) electrode shows two

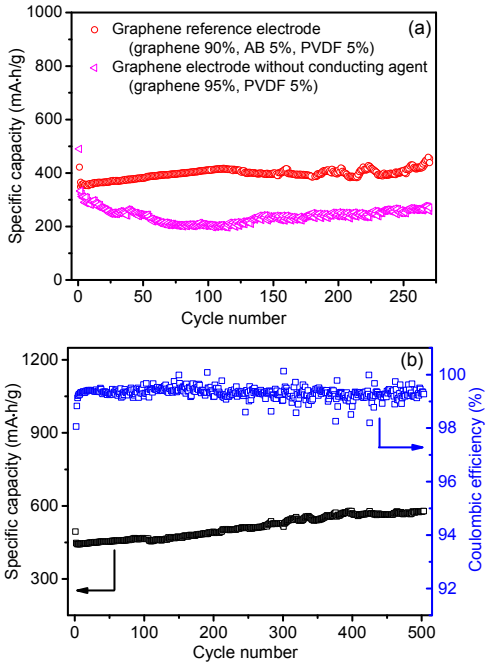

Fig. 5 Cycling performance of graphene electrode prepared without conducting agent and graphene reference electrode (a) and of GMC (8:2) electrode over 500 cycles (b)

peaks at 1.15 and 1.5 V; similar peaks occur on the cathodic scan of reference graphene and MCMB electrodes around 0.9 V for reference electrodes. These can be attributed to SEI formation and are in a good correlation with charge/discharge curves. The reduction peak at 0.01 V appears to be due to lithium intercalation into the active material. Oxidation peaks in the anodic scan at 0.25 V for the GMC electrode and at 0.6 V for reference electrodes are attributed to lithium extraction from the active material. A significant rise in current values along with the decreased potential difference between oxidation and reduction peaks for the GMC (8:2) electrode in comparison with the graphene and MCMB ones indicates a more effective lithium storage mechanism. As presented in Fig. 6b, the CV curves of the GMC (8:2) electrode overlap each other indicating the stability of the electrode. Reduction peaks are shifted up for 0.5 mV in the 3rd and 4th cycles due to the activation of new material sites for lithium storage.

To further confirm the structural stability of the GMC (8:2) electrode, one of the cells was disassembled inside an Ar-filled glove box. The electrode was washed with dimethyl carbonate and dried under

vacuum, and its morphology was investigated using SEM (Fig. 7). The electrode had kept the same structure as before cycling, the surface was uniform and homogenous, and no obvious cracks or disintegration were observed.

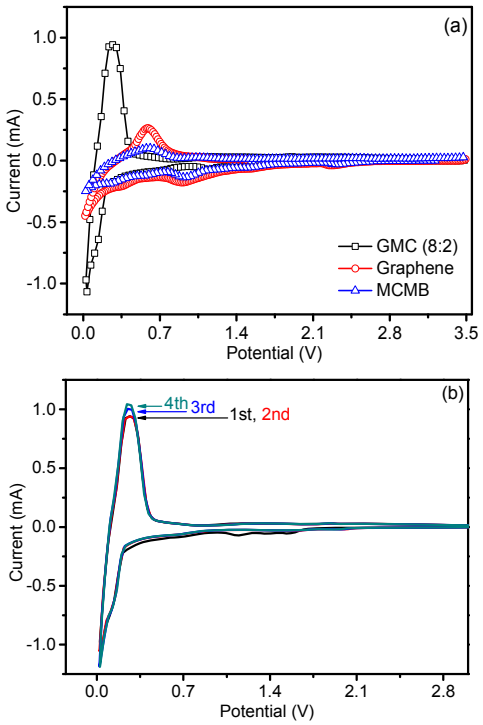

Fig. 6 Cyclic voltammetry curves at a scanning speed of 0.3 mV/s for GMC (8:2), graphene, and MCMB electrodes at the first cycle (a) and GMC (8:2) electrode for four cycles (b)

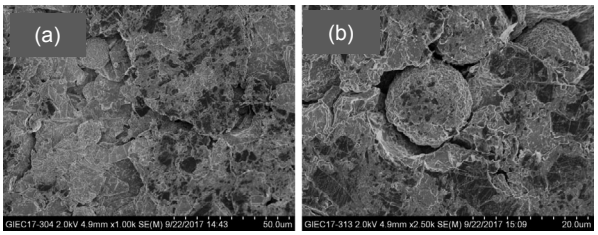

Fig. 7 SEM images of the GMC (8:2) electrode after 200 cycles at magnifications of 1000 (a) and 2500 (b)

Electrochemical impedance spectroscopy brings further understanding of electrode kinetics (Fig. 8). The intercept of impedance spectra with the Z' axis gives the ohmic resistance R_s—the sum of electrolyte, separator, and electrical contact resistance; the semicircle in the high-to-middle frequency region corresponds to charge transfer impedance on the electrode/electrolyte interface (R_{CT}), and the inclined line in the low-frequency range represents Li-ion diffusion in a bulk material, or the so-called Warburg resistance (W_1). CPE_{CT} indicates the electrical double layer resistance (Huang et al., 2012). The solution resistance R_s has similar values for the GMC (8:2) (2.857 Ω), graphene reference electrode (3.191 Ω), and MCMB reference electrode (3.62 Ω). Nevertheless, the charge transfer resistance R_{CT} differs among samples and had a minimum value of 32.8 Ω for the GMC (8:2) electrode, which is distinctly less than 76.79 Ω for the graphene reference electrode, and 240 Ω for the MCMB reference electrode, which proves the advantageous kinetics of the GMC electrode.

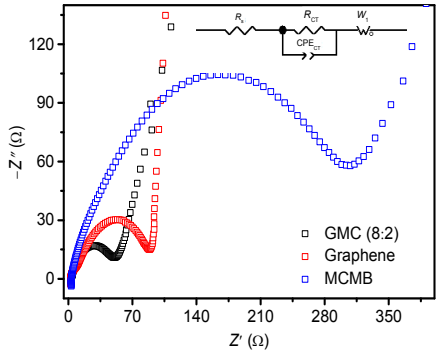

Fig. 8 EIS of the GMC (8:2), graphene, and MCMB reference electrodes

4 Conclusions

In summary, we firstly present a graphene and MCMB composite as an anode material for LIBs. The combination of MCMB with spherical morphology and excellent cycling stability with highly-conductive home-made graphene can effectively prevent the aggregation of graphene sheets and facilitates close-packing of the graphene/MCMB composite electrode (denoted as GMC). GMC (8:2) shows improved cycling stability and rate capability, delivering a high initial charge/discharge capacity of 421.4 mA·h/g/494.8 mA·h/g as well as an excellent capacity retention of over 500 cycles at a current density of 40 mA/g. This improved electrode structure has potential application in LIBs.

Contributors

Inna SMOLIANOVA conducted research and prepared the paper; Jin-long HU and Xin-yue ZHAO helped for guidance of

partial electrochemical tests; Viacheslav DEMENTIEV donated the graphene sample and initialized the collaboration of this research; Ling-zhi ZHANG is responsible for all the research and the publication of the paper including revision of manuscript and all communication during the whole process.

Conflict of interest

Inna SMOLIANOVA, Jin-long HU, Xin-yue ZHAO, Viacheslav DEMENTIEV, and Ling-zhi ZHANG declare that they have no conflict of interest.

References

Alcántara R, Fernández Madrigal FJ, Lavela P, et al., 2000. Characterisation of mesocarbon microbeads (MCMB) as active electrode material in lithium and sodium cells. *Carbon*, 38(7):1031-1041. https://doi.org/10.1016/S0008-6223(99)00215-8

Allen MJ, Tung VC, Kaner RB, 2010. Honeycomb carbon: a review of graphene. *Chemical Reviews*, 110(1):132-145. https://doi.org/10.1021/cr900070d

Birrozzi A, Maroni F, Raccichini R, et al., 2015. Enhanced stability of SnSb/graphene anode through alternative binder and electrolyte additive for lithiumion batteries application. *Journal of Power Sources*, 294:248-253. https://doi.org/10.1016/j.jpowsour.2015.06.065

Cai MZ, Thorpe D, Adamson DH, et al., 2012. Methods of graphite exfoliation. *Journal of Materials Chemistry*, 22(48):24992-25002. https://doi.org/10.1039/c2jm34517j

Cai XY, Lai LF, Shen ZX, et al., 2017. Graphene and graphene-based composites as Li-ion battery electrode materials and their application in full cells. *Journal of Materials Chemistry A*, 5(30):15423-15446. https://doi.org/10.1039/C7TA04354F

Collins J, Gourdin G, Foster M, et al., 2015. Carbon surface functionalities and SEI formation during Li intercalation. *Carbon*, 92:193-244. https://doi.org/10.1016/j.carbon.2015.04.007

Compton OC, Nguyen ST, 2010. Graphene oxide, highly reduced graphene oxide, and graphene: versatile building blocks for carbon-based materials. *Small*, 6(6):711-723. https://doi.org/10.1002/smll.200901934

Dahn JR, Zheng T, Liu YH, et al., 1995. Mechanisms for lithium insertion in carbonaceous materials. *Science*, 270(5236):590-593. https://doi.org/10.1126/science.270.5236.590

Du YH, Tang YF, Huang FQ, et al., 2016. Preparation of three-dimensional free-standing nano-$LiFePO_4$/graphene composite for high performance lithiumion battery. *RSC Advances*, 6(57):52279-52283. https://doi.org/10.1039/c6ra08937b

Dunn B, Kamath H, Tarascon JM, 2011. Electrical energy storage for the grid: a battery of choices. *Science*, 334(6058):928-935. https://doi.org/10.1126/science.1212741

Guo P, Song HH, Chen XH, 2009. Electrochemical performance of graphene nanosheets as anode material for lithium-ion batteries. *Electrochemistry Communications*, 11(6):1320-1324. https://doi.org/10.1016/j.elecom.2009.04.036

Hu J, Li H, Huang XJ, 2007. Electrochemical behavior and microstructure variation of hard carbon nano-spherules as anode material for Li-ion batteries. *Solid State Ionics*, 178(3-4):265-271. https://doi.org/10.1016/j.ssi.2006.12.014

Huang X, Zeng ZY, Fan ZX, et al., 2012. Graphene-based electrodes. *Advanced Materials*, 24(45):5979-6004. https://doi.org/10.1002/adma.201201587

Imtiaz M, Zhu CL, Li Y, et al., 2017. Functionalized bioinspired porous carbon with graphene sheets as anode materials for lithium-ion batteries. *Journal of Alloys and Compounds*, 724:296-305. https://doi.org/10.1016/j.jallcom.2017.07.005

Jaguemont J, Boulon L, Dubé Y, 2016. A comprehensive review of lithium-ion batteries used in hybrid and electric vehicles at cold temperatures. *Applied Energy*, 164:99-114. https://doi.org/10.1016/j.apenergy.2015.11.034

Li N, Chen ZP, Ren WC, et al., 2012. Flexible graphene-based lithiumion batteries with ultrafast charge and discharge rates. *Proceedings of the National Academy of Sciences of the United States of America*, 109(43):17360-17365. https://doi.org/10.1073/pnas.1210072109

Li Z, Li GY, Ouyang J, et al., 2019. Defective lithium storage boosts high rate and long-life span of carbon fibers. *ChemistrySelect*, 4(19):5768-5775. https://doi.org/10.1002/slct.201901140

Linden D, Reddy TB, 2002. Handbook of Batteries, 3rd Edition. McGraw-Hill, New York, USA.

Liu HL, Tang YF, Zhao W, et al., 2018. Facile synthesis of nitrogen and halogen dual-doped porous graphene as an advanced performance anode for lithium-ion batteries. *Advanced Materials Interfaces*, 5(5):1701261. https://doi.org/10.1002/admi.201701261

Mochida I, Korai Y, Ku CH, et al., 2000. Chemistry of synthesis, structure, preparation and application of aromatic-derived mesophase pitch. *Carbon*, 38(2):305-328. https://doi.org/10.1016/s0008-6223(99)00176-1

Novoselov KS, Geim AK, Morozov SV, et al., 2004. Electric field effect in atomically thin carbon films. *Science*, 306(5696):666-669. https://doi.org/10.1126/science.1102896

Ogumi Z, Inaba M, 1998. Electrochemical lithium intercalation within carbonaceous materials: intercalation processes, surface film formation, and lithium diffusion. *Bulletin of the Chemical Society of Japan*, 71(3):521-534. https://doi.org/10.1246/bcsj.71.521

Peled E, Eshkenazi V, Rosenberg Y, 1998. Study of lithium insertion in hard carbon made from cotton wool. *Journal of Power Sources*, 76(2):153-158. https://doi.org/10.1016/S0378-7753(98)00148-7

Qie L, Chen WM, Wang ZH, et al., 2012. Nitrogen-doped

porous carbon nanofiber webs as anodes for lithium ion batteries with a superhigh capacity and rate capability. *Advanced Materials*, 24(15):2047-2050. https://doi.org/10.1002/adma.201104634

Wang BW, Li Z, Zhang JJ, et al., 2019. N-doped 3D interconnected carbon bubbles as anode materials for lithium-ion and sodium-ion storage with excellent performance. *Journal of Nanoscience and Nanotechnology*, 19(11): 7301-7307. https://doi.org/10.1166/jnn.2019.16655

Wang GX, Shen XP, Yao J, et al., 2009. Graphene nanosheets for enhanced lithium storage in lithium ion batteries. *Carbon*, 47(8):2049-2053. https://doi.org/10.1016/j.carbon.2009.03.053

Wang H, Abe T, Maruyama S, et al., 2005. Graphitized carbon nanobeads with an onion texture as a lithium-ion battery negative electrode for high-rate use. *Advanced Materials*, 17(23):2857-2860. https://doi.org/10.1002/adma.200500320

Wang JG, Jin DD, Zhou R, et al., 2016. Highly flexible graphene/Mn_3O_4 nanocomposite membrane as advanced anodes for Li-ion batteries. *ACS Nano*, 10(6):6227-6234. https://doi.org/10.1021/acsnano.6b02319

Wang W, Guo SR, Ozkan M, et al., 2013. Chrysanthemum like carbon nanofiber foam architectures for supercapacitors. *Journal of Materials Research*, 28(7):912-917. https://doi.org/10.1557/jmr.2012.412

Wang ZX, Huang XJ, Xue RJ, et al., 1999. A new possible mechanism of lithium insertion and extraction in low-temperature pyrolytic carbon electrode. *Carbon*, 37(4): 685-692. https://doi.org/10.1016/S0008-6223(98)00245-0

Welna DT, Qu LT, Taylor BE, et al., 2011. Vertically aligned carbon nanotube electrodes for lithium-ion batteries. *Journal of Power Sources*, 196(3):1455-1460. https://doi.org/10.1016/j.jpowsour.2010.08.003

Wu YP, Zhang TF, Zhang F, et al., 2012. In situ synthesis of graphene/single-walled carbon nanotube hybrid material by arc-discharge and its application in supercapacitors. *Nano Energy*, 1(6):820-827. https://doi.org/10.1016/j.nanoen.2012.07.001

Wu ZS, Ren WC, Xu L, et al., 2011. Doped graphene sheets as anode materials with superhigh rate and large capacity for lithiumion batteries. *ACS Nano*, 5(7):5463-5471. https://doi.org/10.1021/nn2006249

Yao J, Wang GX, Ahn JH, et al., 2003. Electrochemical studies of graphitized mesocarbon microbeads as an anode in lithium-ion cells. *Journal of Power Sources*, 114(2):292-297. https://doi.org/10.1016/S0378-7753(02)00585-2

Yoo E, Kim J, Hosono E, et al., 2008. Large reversible Li storage of graphene nanosheet families for use in rechargeable lithiumion batteries. *Nano Letters*, 8(8):2277-2282. https://doi.org/10.1021/nl800957b

Yun YS, Le VD, Kim H, et al., 2014. Effects of sulfur doping on graphene-based nanosheets for use as anode materials in lithium-ion batteries. *Journal of Power Sources*, 262: 79-85. https://doi.org/10.1016/j.jpowsour.2014.03.084

Zhao JF, Wen XM, Xu HS, et al., 2019. Salting-out and salting-in of protein: a novel approach toward fabrication of hierarchical porous carbon for energy storage application. *Journal of Alloys and Compounds*, 788:397-406. https://doi.org/10.1016/j.jallcom.2019.02.252

Zhu S, Li JJ, Ma LY, et al., 2016. Three-dimensional network of N-doped carbon ultrathin nanosheets with closely packed mesopores: controllable synthesis and application in electrochemical energy storage. *ACS Applied Materials & Interfaces*, 8(18):11720-11728. https://doi.org/10.1021/acsami.6b02386

Zhu YW, Murali S, Cai WW, et al., 2010. Graphene and graphene oxide: synthesis, properties, and applications. *Advanced Materials*, 22(35):3906-3924. https://doi.org/10.1002/adma.201001068

中文概要

题　目：高容量石墨烯/中间相碳微球负极材料设计及性能研究

目　的：电动汽车和大规模储能的发展对锂离子电池的能量密度提出了更高的要求，但现有商业石墨负极容量难以满足要求。本文结合石墨烯高电导和高容量的优点以及中间相碳微球材料循环稳定性优良的优势，研究和报道一种容量高和循环性能好的石墨烯/中间相碳微球复合负极材料。

方　法：1. 通过选择高电导率石墨烯和中间相碳微球，制备石墨烯和中间相碳微球复合负极材料。2. 选用商业聚偏氟乙烯（PVDF）粘结剂，制备复合材料电极极片，测试和表征电极的形貌、电导以及半电池的充放电等电化学性能，并优化复合材料质量比。3. 选择优化的复合负极材料（GMC (8:2)），研究其长循环性能。

结　论：中间相碳微球的球形结构能有效防止石墨烯的折叠团聚，从而发挥石墨烯的高电导性能。因此，石墨烯/中间相碳微球复合负极材料表现出了很好的倍率性能和循环性能，且其容量达到了421 mA·h/g 以上，高于商业石墨的理论容量，具有潜在的应用前景。

关键词：石墨烯；中间相碳微球；负极材料；锂离子电池